HHS Public Access

Author manuscript

J Am Chem Soc. Author manuscript; available in PMC 2015 November 30.

Published in final edited form as:

J Am Chem Soc. 2015 October 28; 137(42): 13480–13483. doi:10.1021/jacs.5b09014.

Measuring Residual Dipolar Couplings in Excited Conformational States of Nucleic Acids by CEST NMR Spectroscopy

Bo Zhao[†,‡] and **Qi Zhang**[†,*]

[†]Department of Biochemistry and Biophysics, University of North Carolina at Chapel Hill, Chapel Hill, North Carolina 27599, United States

[‡]Department of Chemistry, University of North Carolina at Chapel Hill, Chapel Hill, North Carolina 27599, United States

Abstract

Nucleic acids undergo structural transitions to access sparsely populated and transiently lived conformational states—or excited conformational states—that play important roles in diverse biological processes. Despite ever-increasing detection of these functionally essential states, 3D structure determination of excited states (ESs) of RNA remains elusive. This is largely due to challenges in obtaining high-resolution structural constraints in these ESs by conventional structural biology approaches. Here, we present nucleic-acid-optimized chemical exchange saturation transfer (CEST) NMR spectroscopy for measuring residual dipolar couplings (RDCs), which provide unique long-range angular constraints in ESs of nucleic acids. We demonstrate these approaches on a fluoride riboswitch, where one-bond ^{13}C-^{1}H RDCs from both base and sugar moieties provide direct structural probes into an ES of the ligand-free riboswitch.

Nucleic acids are highly dynamic entities that undergo conformational transitions to access distinct states with unique structural and kinetic properties required for function.[1] In recent decades, tremendous progress in determining high-resolution RNA structures by X-ray crystallography and NMR spectroscopy has significantly advanced our understanding of the chemical basis for diverse non-coding RNA functions. While these high-resolution structural studies have primarily focused on functional states that are highly populated and long-lived, it is increasingly recognized that many functionally essential states are sparsely populated and transiently lived.[1] Determining high-resolution structures of these states—or excited conformational states—of RNA remains a major experimental obstacle to structural biology, as they often exist in insufficient abundance and for too little time to be studied by conventional structural biology approaches.[2]

[*]Corresponding Author. zhangqi@unc.edu.

ASSOCIATED CONTENT

Supporting Information

The Supporting Information is available free of charge on the ACS Publications website at DOI: 10.1021/jacs.5b09014.

Details of experiments and data analysis (PDF)

The authors declare no competing financial interest.

NMR spectroscopy has been a powerful tool for structural and dynamic studies of nucleic acids.[2] Recent developments in nucleic-acid NMR, including conventional $R_{1\rho}$ relaxation dispersion (RD),[3] Carr-Purcell-Meiboom-Gill (CPMG) RD,[4] low spin-lock field $R_{1\rho}$ RD,[5] and chemical exchange saturation transfer (CEST) spectroscopy,[6] have opened avenues for characterizing excited states (ESs) of RNA that are "invisible" to conventional NMR experiments, where not only their thermodynamics and kinetics can be quantified but also their structural properties can be inferred with extracted NMR chemical shifts. The rich structural information encompassed in chemical shifts[7] offers an exciting strategy for *de novo* determination of secondary structures of excited RNA states[5e] and, given recent progress in ^{1}H chemical shift guided computational prediction of 3D RNA structures,[8] makes it feasible for tertiary structure determination of excited RNA states. However, since the relation between chemical shifts and high-resolution RNA structures remains semiempirical,[7] it is also of particular interest and importance to obtain direct structural constraints to facilitate atomic-resolution structure determination of ESs of RNA. While direct bond orientation constraints have been obtained for determining excited protein structures[9] via the measurement of residual dipolar couplings (RDCs)[10] using CPMG RD experiments,[11] applying these CPMG methods to nucleic acids without specific labeling schemes[4] can be complicated due to the presence of extensive ^{13}C-^{13}C scalar couplings in uniformly labeled systems.[12]

In recent years, the saturation transfer type of NMR experiment[13] has become a powerful approach for studying ESs in biomolecules, including protofibrils,[14] proteins,[15] and RNA.[6] By avoiding complications due to ^{13}C-^{13}C scalar couplings,[16] CEST NMR has accurately characterized populations, lifetimes, and chemical shifts of ESs in uniformly ^{13}C/^{15}N-labeled proteins[15b,c] and RNA.[6] Here, we present two CEST NMR approaches that measure ^{13}C-^{1}H splittings to obtain one-bond ^{13}C-^{1}H RDCs, a type of NMR measurement that provides unique valuable long-range angular constraints for RNA structure determination by NMR,[17] in bases and sugars of RNA ESs.

The first approach, based on our nucleic-acid-optimized ^{13}C HSQC CEST experiment,[6] employs a recently developed scheme for measuring scalar couplings in ESs of proteins.[15d] Here, the key is to turn off ^{1}H decoupling during the chemical exchange period (T_{EX}) in the conventional HSQC CEST experiment (Figure S1), allowing ^{13}C multiplet structures to develop due to large one-bond ^{13}C-^{1}H scalar couplings ($^{1}J_{CH} \approx 200$ Hz) in the CEST profiles. To demonstrate this approach, we carried out CEST measurements on a guanosine ^{13}C/^{15}N-labeled *Bacillus cereus* fluoride riboswitch,[18] which regulates the transcription of fluoride transporters. Recently, we discovered that the ligand-free fluoride riboswitch undergoes a conformational exchange between an unfolded ground state (GS) and a potential pseudoknot-like ES, where the P1 apical loop and the unfolded 3′ tail transiently form the ES P3 stem that is essential for gene regulation (Figure 1A).[6] Figure 1B shows representative ^{13}C HSQC CEST profiles measured in the ligand-free riboswitch in isotropic solution. For G33, a P2 stem residue that has no conformational exchange, single GS intensity dips in the conventional ^{1}H-decoupled CEST profiles split into two dips in the absence of ^{1}H decoupling, separated by GS $^{1}J_{C8H8}$ and $^{1}J_{C1'H1'}$ couplings for base (C8) and sugar (C1′) profiles, respectively. For P1 loop residue G10, which transitions between the

two states, both GS and ES intensity dips in the conventional profiles split, resulting in four apparent dips in the ^{1}H-coupled profiles, where splittings between each pair correspond to $^{1}J_{CH}$ couplings in GS and ES, respectively. Next, the same set of experiments was carried out in the presence of 9.7 mg/mL Pf1 phage alignment media (Figure 1C). Here, while the ^{13}C-^{1}H HSQC spectra recorded in the absence and presence of Pf1 phage overlap excellently (Figure S2), dipolar couplings, due to the RNA being partially aligned, are no longer averaged to zero, resulting in splittings between pairs of dips in the ^{1}H-coupled profiles equal to the sum of $^{1}J_{CH}$ and one-bond ^{13}C-^{1}H RDCs ($^{1}D_{CH}$). Hence, $^{1}D_{CH}$'s of GS and ES can be determined by taking the difference between corresponding ^{13}C-^{1}H splittings in isotropic and partially aligned conditions, which can be quantitatively extracted by fitting their CEST profiles with the Bloch-McConnell equation[19] that describes magnetization evolution in a coupled two-spin ^{13}C-^{1}H system (see the SI).

Since ES RDCs cannot be measured directly for cross-validation, the accuracy of this approach was first examined by extracting GS $^{1}D_{CH}$ values from CEST profiles, which can be compared to values measured directly via conventional methods[17b] (Table S1). For all guanosine residues from the stable P2 stem, GS ^{13}C-^{1}H splittings were extracted by fitting their individual sets of CEST profiles to a simple one-state model (Figures 1B,C and S3 and Table S2). While other guanosine residues displayed either multiple or asymmetrically broadened intensity dips in their conventional CEST profiles as described previously,[6] proper analysis of these complex profiles with a unified exchange model requires a thorough understanding of the underlying global and/or local conformational transitions, which are currently being investigated. Here, to establish the validity of this approach in measuring ES RDCs, we focus on G8 and G10, the two central residues of the ES P3 stem, which have been shown to undergo a global conformational transition between the unfolded GS and the pseudoknot-like ES.[6] To extract GS and ES $^{1}J_{CH}$ values of G8 and G10, all of their base and sugar CEST profiles measured in isotropic solution were globally fit to a single two-state exchange model. Similarly, all of their profiles measured in Pf1 phage were globally fit to extract GS and ES $^{1}J_{CH}$+$^{1}D_{CH}$ values (Figures 1B,C and S3 and Table S2). The resulting global exchange parameters showed overall good agreement, where rate of exchange (k_{ex} = k_{GE}+k_{EG}) and ES population (p_{ES}) are 108±5 s^{-1} and 9.4±0.1% for the isotropic sample and 88±5 s^{-1} and 10.1±0.2% for the partially aligned samples (Table S3). More importantly, the obtained GS-ES chemical shift differences ($\Delta\varpi = \varpi_{ES} - \varpi_{GS}$) agree very well between the two conditions (Table S3). For example, for C8 of G10, $\Delta\varpi$(iso) = −3.98±0.01 ppm is essentially the same as $\Delta\varpi$(phage) = −4.00±0.01 ppm. Together, these results strongly suggest that not only does Pf1 phage not affect GS and ES structures, it also minimally perturbs the conformational exchange of the ligand-free riboswitch.

Figure 2A,B compares GS ^{13}C-^{1}H splittings of G8, G10, and P2 G residues extracted from HSQC CEST profiles and those measured directly. Good agreement was observed, with root-mean-square deviations (RMSDs) between the two methods being 1.5 and 2.4 Hz for isotropic and partially aligned samples, respectively. GS $^{1}D_{CH}$ values were then calculated by subtracting GS $^{1}J_{CH}$ from GS $^{1}J_{CH}$+$^{1}D_{CH}$, which, as expected, agree very well between the two methods, with RMSD = 2.0 Hz (Figure 2C). It is worth noting that, despite the presence of large C1′-C2′couplings in the sugar moiety, accurate $^{1}J_{C1'H1'}$ and $^{1}D_{C1'H1'}$

values can be obtained. After establishing this approach in measuring GS $^1D_{CH}$, ES base and sugar $^1D_{CH}$'s of G8 and G10 were calculated as the difference between their extracted $^1J_{CH}$ and $^1J_{CH}+^1D_{CH}$ (Table S2). While detailed ES structural analysis with RDCs requires not only additional measurements but also a critical treatment of the coupling between internal motions and overall alignment[20] (a spectroscopy property that often renders structural and dynamic characterization of flexible nucleic acids intractable), the obtained ES $^1D_{CH}$'s of G8 and G10 do provide direct insights to support some ES structural features of the riboswitch. First, in the GS, both G8 and G10 are located in the P1 apical loop, which is flexible and largely unfolded. This structural property is reflected by small $^1D_{CH}$'s across their bases and sugars, ranging from 1 to 8 Hz. In contrast, in the ES, both residues fold into a helical conformation as part of the P3 stem, whose local flexibility would be significantly reduced. Consistent with this expectation, much larger ES $^1D_{CH}$'s were observed, ranging from −22 to 20 Hz. Further, as can be seen (Figure 2D), ES $^1D_{CH}$'s of G8 and G10 showed almost no correlation with their GS counterparts, strongly indicating that the ES P3 stem has an orientation relative to the external magnetic field that is dramatically different from that of the unfolded P1 apical loop in the ground-state conformation.

With the first approach, we show that GS $^1D_{CH}$ can be accurately determined by CEST spectroscopy, and ES $^1D_{CH}$ for residues undergoing conformational exchange can also be measured simultaneously. To independently validate those extracted ES $^1D_{CH}$'s, we developed an alternative CEST approach for RDC measurement, where TROSY (transverse relaxation optimized spectroscopy)[21a] and anti-TROSY components of GS/ES ^{13}C magnetizations are individually measured for quantifying GS and ES ^{13}C-^{1}H splittings. The nucleic-acid-optimized ^{13}C TROSY/anti-TROSY-selected (TS/aTS) CEST experiments (Figure S4) were built upon elegant schemes in TS $R_{1\rho}$ RD,[21b] CPMG RD RDC,[11b] TS ^{15}N CEST,[15e] and nucleic-acid-optimized TROSY-detected $R_{1\rho}$ spin relaxation[21c] experiments. Key experimental elements are briefly described here. First, TROSY or anti-TROSY ^{13}C magnetization is selected via an S^{3}E filter[21d] prior to T_{EX}. Second, during T_{EX}, an S^{3}CT selective-inversion element[21e] is employed to suppress cross-relaxation between TROSY and anti-TROSY components. Third, a ^{1}H 180° pulse is applied after T_{EX} in the aTS experiment to convert anti-TROSY to TROSY ^{13}C magnetization, resulting in TROSY spectra with better resolution and enhanced sensitivity while reporting on exchange between anti-TROSY ^{13}C magnetizations.[11b]

Figure 3A,B shows representative ^{13}C TS/aTS CEST profiles of G10 measured in isotropic and partially aligned conditions. Overall the shapes observed were similar to the conventional ^{1}H-decoupled HSQC CEST profiles (Figure 1), which display two intensity dips, one each for GS and ES. However, positions of these dips in TS/aTS profiles are downfield and upfield shifted relative to those observed in the conventional profile, respectively, which correspond to chemical shifts of TROSY and anti-TROSY ^{13}C magnetizations of GS and ES. To determine distances between pairs of TROSY and anti-TROSY intensity dips, hence values of $^1J_{CH}$ or $^1J_{CH}+^1D_{CH}$, TS/aTS CEST profiles can be jointly fit using the same Bloch-McConnell equation for a coupled two-spin ^{13}C-^{1}H system (see the SI).

To this end, we analyzed ^{13}C TS/aTS CEST profiles using the same procedure as described for ^{13}C HSQC CEST data (Figures 3A,B and S5 and Table S4). Specifically, GS splittings of all P2 guanosine residues were extracted by fitting each individual set of TS/aTS profiles to a single-state model. GS and ES splittings for G8 and G10 were simultaneously extracted by global fitting of all their isotropic (partially aligned) TS/aTS profiles to a single two-state exchange model. The GS $^1J_{CH}$, $^1J_{CH}+^1D_{CH}$, and $^1D_{CH}$ values extracted from TS/aTS CEST profiles agree very well with those measured directly, establishing the validity of this approach in measuring GS $^1D_{CH}$ (Figures 3C and S6). ES $^1D_{CH}$'s of G8 and G10 were then calculated based on extracted ES $^1J_{CH}$ and $^1J_{CH}+^1D_{CH}$. This independent set of ES $^1D_{CH}$'s agrees well with those determined in the first approach, with RMSD = 4.0 Hz, similar to experimental errors (Figure 3D). Numerical simulations further indicate that this approach can be reliably extended to relatively large systems (Figure S7). It is also worth noting that the TS/aTS CEST experiments accurately characterize the conformational exchange in the ligand-free riboswitch (Table S5). The resulting global exchange parameters (k_{ex}(iso) = 110±9 s^{-1} and p_{ES}(iso) = 9.0±0.2%) as well as ES chemical shifts ($\Delta\varpi$(iso) = −3.99±0.01 ppm for C8 of G10) are in excellent agreement with those obtained from conventional HSQC CEST experiment. Thus, these two CEST approaches cross-validate each other as means to accurately quantify conformational transitions and determine ES RDCs of nucleic acids. One final note is that, while G8 and G10 do not benefit from the TROSY effect due to their intrinsic high flexibilities, TROSY-based experiments can be valuable for large RNAs, offering enhanced sensitivity and more accurate characterization of the dynamic process by measuring the contribution of chemical exchange to the narrow TROSY ^{13}C magnetization.[21b,c]

In summary, we have presented two approaches based on ^{13}C CEST NMR spectroscopy for measuring residual dipolar couplings, hence long-range angular constraints, in sparsely populated and transiently lived conformational states of nucleic acids, which in principle can also be adapted for proteins. The set of HSQC- and TROSY-based CEST methods provides a versatile approach for characterizing excited states of nucleic acids across a wide range of molecular weights, where not only direct structural constraints in terms of RDCs but also empirical structural constraints using chemical shifts can be simultaneously obtained. It has become increasingly clear that nucleic acids are highly dynamic entities that sample excited conformational states with distinct functional roles.[1] A deep mechanistic understanding of these fascinating nucleic acid functions requires comprehensive structural knowledge of their diverse conformational states. The experimental approaches presented here, along with developments in secondary structure determination of RNA ES[5e] and chemical-shift-guided 3D RNA structure prediction,[8] pave a way for *de novo* high-resolution structure determination of functional excited states of nucleic acids.

Supplementary Material

Refer to Web version on PubMed Central for supplementary material.

ACKNOWLEDGMENTS

We thank Dr. Greg Young for maintenance of the NMR instruments. This work was supported by start-up fund from the University of North Carolina at Chapel Hill and grants from the March of Dimes Foundation (5-FY12-561) and NIH (R01 GM114432).

REFERENCES

1. Dethoff EA, Chugh J, Mustoe AM, Al-Hashimi HM. Nature. 2012; 482:322. [PubMed: 22337051]
2. (a) Rinnenthal J, Buck J, Ferner J, Wacker A, Furtig B, Schwalbe H. Acc. Chem. Res. 2011; 44:1292. [PubMed: 21894962] (b) Bothe JR, Nikolova EN, Eichhorn CD, Chugh J, Hansen AL, Al-Hashimi HM. Nat. Methods. 2011; 8:919. [PubMed: 22036746]
3. (a) Hoogstraten CG, Wank JR, Pardi A. Biochemistry. 2000; 39:9951. [PubMed: 10933815] (b) Blad H, Reiter NJ, Abildgaard F, Markley JL, Butcher SE. J. Mol. Biol. 2005; 353:540. [PubMed: 16181635] (c) Shajani Z, Varani G. J. Mol. Biol. 2005; 349:699. [PubMed: 15890361]
4. (a) Johnson JE Jr, Hoogstraten CG. J. Am. Chem. Soc. 2008; 130:16757. [PubMed: 19049467] (b) Kloiber K, Spitzer R, Tollinger M, Konrat R, Kreutz C. Nucleic Acids Res. 2011; 39:4340. [PubMed: 21252295] (c) Wunderlich CH, Spitzer R, Santner T, Fauster K, Tollinger M, Kreutz C. J. Am. Chem. Soc. 2012; 134:7558. [PubMed: 22489874]
5. (a) Massi F, Johnson E, Wang C, Rance M, Palmer AG III. J. Am. Chem. Soc. 2004; 126:2247. [PubMed: 14971961] (b) Korzhnev DM, Orekhov VY, Kay LE. J. Am. Chem. Soc. 2005; 127:713. [PubMed: 15643897] (c) Hansen AL, Nikolova EN, Casiano-Negroni A, Al-Hashimi HM. J. Am. Chem. Soc. 2009; 131:3818. [PubMed: 19243182] (d) Nikolova EN, Kim E, Wise AA, O'Brien PJ, Andricioaei I, Al-Hashimi HM. Nature. 2011; 470:498. [PubMed: 21270796] (e) Dethoff EA, Petzold K, Chugh J, Casiano-Negroni A, Al-Hashimi HM. Nature. 2012; 491:724. [PubMed: 23041928]
6. Zhao B, Hansen AL, Zhang Q. J. Am. Chem. Soc. 2014; 136:20. [PubMed: 24299272]
7. (a) Dejaegere A, Bryce RA, Case DA. ACS Symp. Ser. 1999; 732:194.(b) Cromsigt JA, Hilbers CW, Wijmenga SS. J. Biomol. NMR. 2001; 21:11. [PubMed: 11693565] (c) Fares C, Amata I, Carlomagno T. J. Am. Chem. Soc. 2007; 129:15814. [PubMed: 18052161] (d) Barton S, Heng X, Johnson BA, Summers MF. J. Biomol. NMR. 2013; 55:33. [PubMed: 23180050]
8. (a) Frank AT, Horowitz S, Andricioaei I, Al-Hashimi HM. J. Phys. Chem. B. 2013; 117:2045. [PubMed: 23320790] (b) Sripakdeevong P, Cevec M, Chang AT, Erat MC, Ziegeler M, Zhao Q, Fox GE, Gao X, Kennedy SD, Kierzek R, Nikonowicz EP, Schwalbe H, Sigel RK, Turner DH, Das R. Nat. Methods. 2014; 11:413. [PubMed: 24584194]
9. Korzhnev DM, Religa TL, Banachewicz W, Fersht AR, Kay LE. Science. 2010; 329:1312. [PubMed: 20829478]
10. (a) Tolman JR, Flanagan JM, Kennedy MA, Prestegard JH. Proc. Natl. Acad. Sci. U.S.A. 1995; 92:9279. [PubMed: 7568117] (b) Tjandra N, Bax A. Science. 1997; 278:1111. [PubMed: 9353189]
11. (a) Igumenova TI, Brath U, Akke M, Palmer AG III. J. Am. Chem. Soc. 2007; 129:13396. [PubMed: 17929930] (b) Vallurupalli P, Hansen DF, Stollar E, Meirovitch E, Kay LE. Proc. Natl. Acad. Sci. U.S.A. 2007; 104:18473. [PubMed: 18006656]
12. Lundstrom P, Hansen DF, Kay LE. J. Biomol. NMR. 2008; 42:35. [PubMed: 18762869]
13. Forsen S, Hoffman RA. J. Chem. Phys. 1963; 39:2892.
14. Fawzi NL, Ying J, Ghirlando R, Torchia DA, Clore GM. Nature. 2011; 480:268. [PubMed: 22037310]
15. (a) Vallurupalli P, Bouvignies G, Kay LE. J. Am. Chem. Soc. 2012; 134:8148. [PubMed: 22554188] (b) Bouvignies G, Vallurupalli P, Kay LE. J. Mol. Biol. 2014; 426:763. [PubMed: 24211467] (c) Long D, Sekhar A, Kay LE. J. Biomol. NMR. 2014; 60:203. [PubMed: 25348177] (d) Hansen AL, Kay LE. Proc. Natl. Acad. Sci. U.S.A. 2014; 111:E1705. [PubMed: 24733918] (e) Long D, Bouvignies G, Kay LE. Proc. Natl. Acad. Sci. U.S.A. 2014; 111:8820. [PubMed: 24889628]
16. Vallurupalli P, Bouvignies G, Kay LE. ChemBioChem. 2013; 14:1709. [PubMed: 23784752]

17. (a) Hansen MR, Mueller L, Pardi A. Nat. Struct. Biol. 1998; 5:1065. [PubMed: 9846877] (b) Bailor MH, Musselman C, Hansen AL, Gulati K, Patel DJ, Al-Hashimi HM. Nat. Protoc. 2007; 2:1536. [PubMed: 17571061] (c) Tolbert BS, Miyazaki Y, Barton S, Kinde B, Starck P, Singh R, Bax A, Case DA, Summers MF. J. Biomol. NMR. 2010; 47:205. [PubMed: 20549304]

18. Baker JL, Sudarsan N, Weinberg Z, Roth A, Stockbridge RB, Breaker RR. Science. 2012; 335:233. [PubMed: 22194412]

19. McConnell HM. J. Chem. Phys. 1958; 28:430.

20. Zhang Q, Stelzer AC, Fisher CK, Al-Hashimi HM. Nature. 2007; 450:1263. [PubMed: 18097416]

21. (a) Pervushin K, Riek R, Wider G, Wuthrich K. Proc. Natl. Acad. Sci. U.S.A. 1997; 94:12366. [PubMed: 9356455] (b) Igumenova TI, Palmer AG III. J. Am. Chem. Soc. 2006; 128:8110. [PubMed: 16787055] (c) Hansen AL, Al-Hashimi HM. J. Am. Chem. Soc. 2007; 129:16072. [PubMed: 18047338] (d) Meissner A, Duus JO, Sorensen OW. J. Magn. Reson. 1997; 128:92.(e) Sorensen MD, Meissner A, Sorensen OW. J. Biomol. NMR. 1997; 10:181.

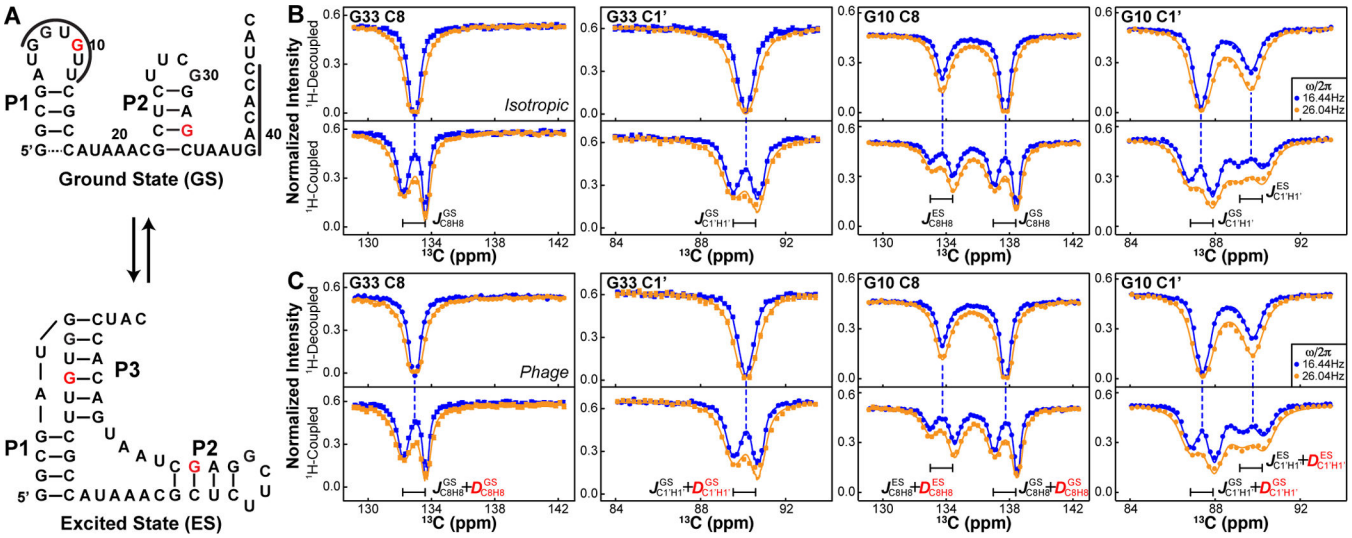

Figure 1.

^{13}C HSQC CEST ^{13}C-^{1}H splittings of the ground state and an "invisible" excited state in the ligand-free *Bacillus cereus* fluoride riboswitch. (A) GS and ES secondary structures of the ligand-free riboswitch. ES P3 residues are outlined in GS. (B,C) Base (C8) and sugar (C1′) ^{13}C HSQC CEST profiles of G33 and G10 measured at ^{13}C B_1 fields of 16.44 (blue) and 26.04 Hz (orange) in the absence (B) and presence (C) of 9.7 mg/mL Pf1 phage alignment media. Solid lines represent best joint-fits of ^{1}H-decoupled and ^{1}H-coupled ^{13}C HSQC CEST profiles.

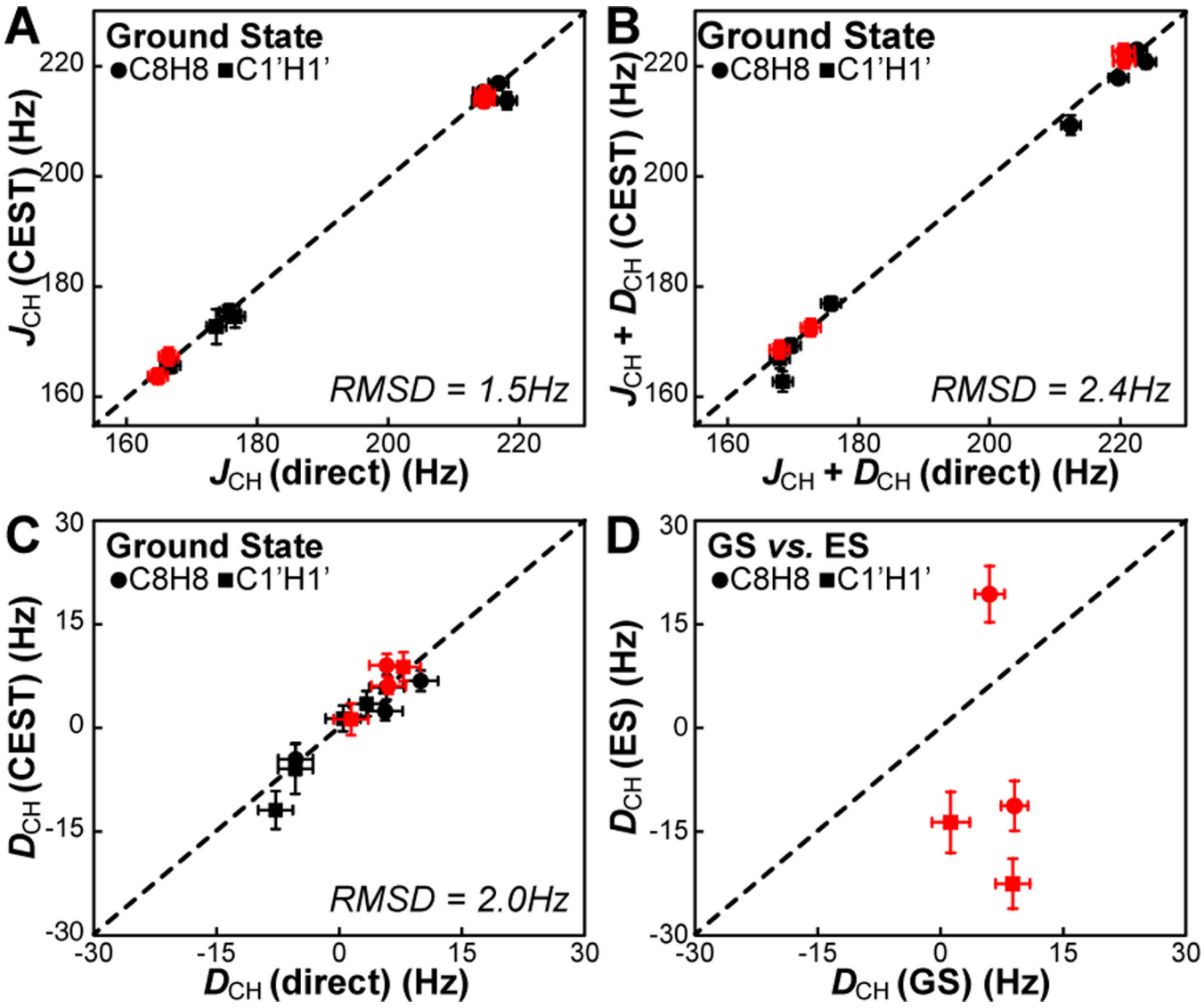

Figure 2.

Measurement of ^{13}C-^{1}H RDCs by ^{13}C HSQC CEST. (A,B) Comparison of ground state (GS) ^{13}C-^{1}H splittings determined from CEST and direct measurements in the absence (A) and presence (B) of 9.7 mg/mL Pf1 phage. (C) GS ^{13}C-^{1}H RDCs ($^{1}D_{CH}$) determined from CEST approach agree well with values measured directly. G8 and G10 are shown in red. (D) Comparison of base and sugar $^{1}D_{CH}$ values of ground and excited states (ES) of G8 and G10.

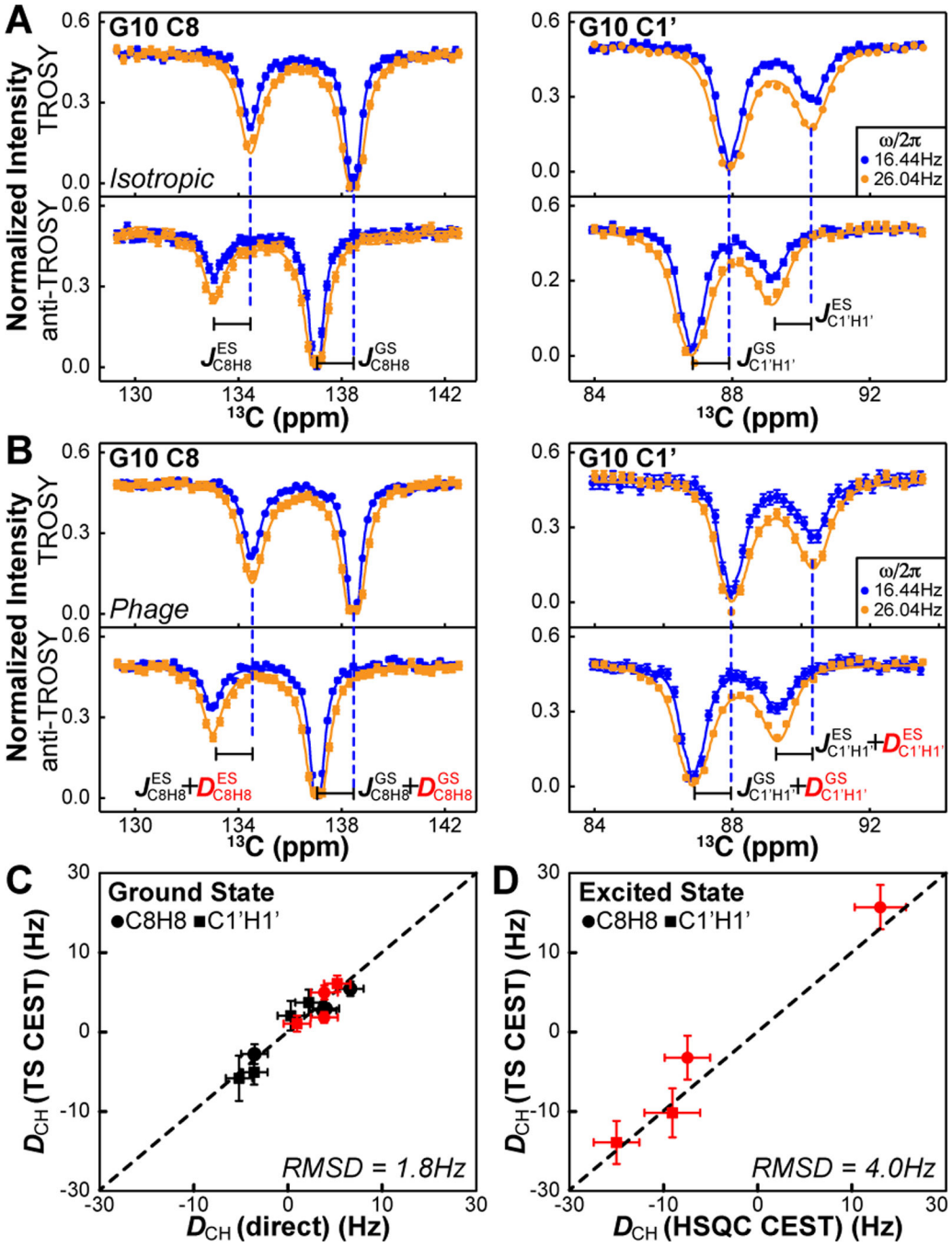

Figure 3.

Measurement of ^{13}C-^{1}H splittings and RDCs of GS and ES in the ligand-free fluoride riboswitch by ^{13}CTROSY/anti-TROSY-selected (TS/aTS) CEST. (A,B) Base (C8) and sugar (C1′) ^{13}C TS/aTS CEST profiles of G10 measured in the absence (A) and presence (B) of Pf1 phage. Solid lines represent best fits of TS/aTS CEST profiles. (C) GS $^{1}D_{CH}$'s agree well between TS/aTS CEST and direct measurements. G8 and G10 shown in red. (D) ES $^{1}D_{CH}$'s ofG8 and G10 agree well between the HSQC and TS/aTS CEST measurements.